High-precision Penning-trap mass measurements of heavy xenon isotopes for nuclear structure studies

D. Neidherr,[1] R. B. Cakirli,[2] G. Audi,[3] D. Beck,[4] K. Blaum,[5] Ch. Böhm,[5] M. Breitenfeldt,[6] R. F. Casten,[7] S. George,[5] F. Herfurth,[4] A. Herlert,[8] A. Kellerbauer,[9] M. Kowalska,[8] D. Lunney,[3] E. Minaya-Ramirez,[3] S. Naimi,[3] M. Rosenbusch,[6] S. Schwarz,[10] and L. Schweikhard[6]

[1]*Johannes Gutenberg-Universität, Institut für Physik, D-55099 Mainz, Germany*
[2]*Department of Physics, Istanbul University, Istanbul, Turkey*
[3]*CSNSM-IN2P3-CNRS, Université de Paris Sud, Orsay, France*
[4]*GSI Helmholtzzentrum für Schwerionenforschung GmbH, D-64291 Darmstadt, Germany*
[5]*Max-Planck-Institut für Kernphysik, D-69117 Heidelberg, Germany*
[6]*Ernst-Moritz-Arndt-Universität, Institut für Physik, D-17487 Greifswald, Germany*
[7]*Wright Nuclear Structure Laboratory, Yale University, New Haven, Connecticut 06520-8120, USA*
[8]*CERN, Physics Department, CH-1211 Geneva 23, Switzerland*
[9]*Commission of European Communities, Joint Research Center, European Institute of Transuranium Elements, D-76125 Karlsruhe, Germany*
[10]*NSCL, Michigan State University, East Lansing, Michigan 48824-1321, USA*

(Received 27 July 2009; published 21 October 2009)

With the double Penning-trap mass spectrometer ISOLTRAP at ISOLDE/CERN the masses of the neutron-rich isotopes $^{136-146}$Xe were measured with a relative uncertainty of the order of 10^{-8} to 10^{-7}. In particular, the masses of $^{144-146}$Xe were measured for the first time. These new mass values allow one to extend calculations of the mass surface in this region. Proton-Neutron interaction strength, obtained from double differences of binding energies, relate to subtle structural effects, such as the onset of octupole correlations, the growth of collectivity, and its relation to the underlying shell model levels. In addition, they provide a test of density functional calculations.

DOI: 10.1103/PhysRevC.80.044323 PACS number(s): 21.10.Dr, 27.60.+j, 32.10.Bi, 21.30.Fe

I. INTRODUCTION

Mass values of exotic nuclei are key parameters for many fields of physics such as nuclear structure research, tests of the standard model, or nuclear astrophysics [1,2]. The binding energy of a nucleus contains the sum of all nuclear forces. Specific effects of nuclear structure can be extracted by the determination of differences of binding energies. One example is the discovery of the so-called "island of inversion" in 1975 [3] from the two-neutron separation energies S_{2n} which did not decrease abruptly at ^{31}Na, as expected for the closed $N = 20$ shell. Moreover, double differences of binding energies can provide filters that isolate particular interactions. Certain filters, such as one that extracts the valence proton-neutron interaction of the last nucleons, can improve our understanding of the evolution of collective behavior in nuclei. In this paper, we will contribute to some of these questions through the measurement of new masses in the $A \sim 140$ mass region.

An important facet of nuclear structure is the evolution of the nuclear shape as a function of the number of neutrons and protons. Nuclei far from closed shells are often deformed, i.e., have nonspherical shapes. Whereas most shapes show a reflection symmetry, some are asymmetric under reflection in their ground states [4]. Such cases are usually investigated via γ-ray spectroscopy of excited nuclei. Low-lying negative-parity states near the ground state, with $E1$ and $E3$ transitions, interleaved with positive-parity states, are normally indicators for stable reflection-asymmetric (i.e., octupole deformed) nuclei.

In this article, we present an alternative approach to revealing octupole deformation effects, which is based on the nuclear binding energies, derived from mass measurements on nine new masses for neutron-rich xenon isotopes, $^{138-146}$Xe, which are relevant for the questions mentioned above. The measurements were carried out with the Penning-trap mass spectrometer ISOLTRAP [5,6] at the CERN Isotope Seperator On-Line (ISOLDE) facility, which produces radioactive ion beams.

Octupole contributions to the binding energy are supposed to be rather small, below 1 or even 0.5 MeV [7,8]. Very often they are hidden by much stronger quadrupolar deformations, which makes it even more difficult to see an effect in the binding energies. Nevertheless, it has been recently shown that there is a much more sensitive link between collective effects in nuclear structure and binding energies than previously assumed [9].

Such a region, relevant to the studies of the proton-neutron interaction where in addition octupole deformation appears, is provided by the lanthanides around ^{146}Ba [10]. To determine the average interaction between the last two neutrons and protons, the masses of two barium ($Z = 56$) and two xenon ($Z = 54$) isotopes have to be well known. Whereas barium masses are measured with an uncertainty of about 10 keV up to ^{144}Ba, the mass values for many of the neutron-rich xenon isotopes were not known or had a very large uncertainty prior to our measurements. In particular, here, we will inspect the double difference of binding energies, called δV_{pn}, that gives the proton-neutron interaction mentioned above, to point out a possible link to octupole correlations and will discuss this quantity as a possible signature for such a degree of freedom.

 ©2009 The American Physical Society

In addition, these empirical proton-neutron interactions have been shown to be closely related to collective correlations on the one hand [11] and to the filling of shell orbits and the overlap of the proton and neutron wave function on the other [12]. We will use the new results here to further study the correlation of large proton-neutron interactions to the growth of collectivity and their dependence on the relative filling of the respective proton and neutron major shells. Finally, we will use the δV_{pn} values obtained for barium nuclei in this study to provide new tests of modern microscopic theories such as those based on density functional calculations [13,14] and to suggest further tests of these calculations.

II. EXPERIMENT

The nuclides of interest were produced at ISOLDE [15] by bombarding a 50 g/cm^2 thick UC_x target with pulses of up to 3×10^{13} protons with an energy of 1.4 GeV from CERN's Proton Synchrotron Booster accelerator. For the present measurements, the nuclear reaction products were guided through a water-cooled transfer line into a newly developed versatile arc discharge ion source (VADIS) [16]. The ionized atoms were accelerated to 30 keV and mass separated with a resolving power of $R = m/\Delta m \approx 4000$ in the ISOLDE high-resolution separator (HRS). The resulting ion beam was injected into the recently installed radio-frequency quadrupole (RFQ) cooler ISCOOL [17] to improve the beam emittance. Afterward, the ions were transported to ISOLTRAP.

Figure 1 shows a sketch of the ISOLTRAP setup. The semicontinuous beam coming from ISOLDE is first injected into a RFQ [19] where the ions are decelerated, cooled, and bunched. After several milliseconds trapping time, the RFQ delivers a low-emittance ion bunch for an ideal injection into the cylindrical preparation Penning trap. Here, a mass-selective buffer-gas cooling technique [20] is applied to detect and separate isobaric contaminations with a typical resolving power in the order of $R = m/\Delta m \approx 10^4$–$10^5$. This procedure is performed for up to a few hundred milliseconds depending on the half-life of the ion of interest and the desired resolution. Figure 2 shows the result of this technique in the case of ^{138}Xe. Here, ^{138}Ba was a candidate for a possible contamination, but in the end, no ^{138}Ba could be observed.

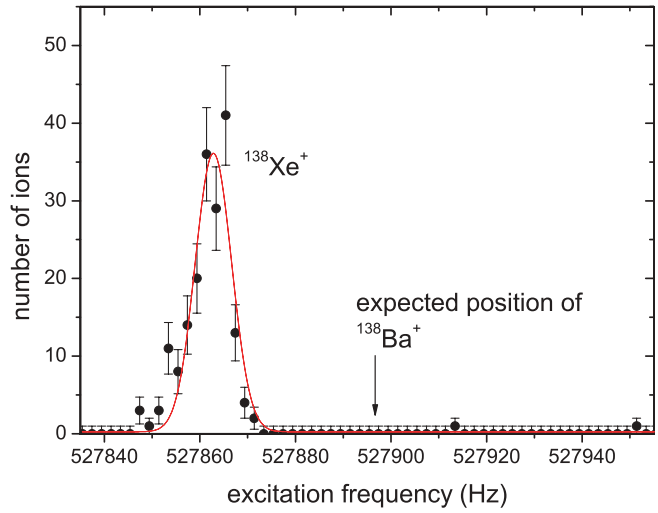

FIG. 2. (Color online) Cooling resonance in the preparation trap in the region of ^{138}Xe. The quadrupolar excitation was applied for 200 ms, resulting in a resolving power $R = m/\Delta m$ of approximately 74 000. Obviously, no ^{138}Ba contamination within the detection limit accompanied the ^{138}Xe beam from ISOLDE.

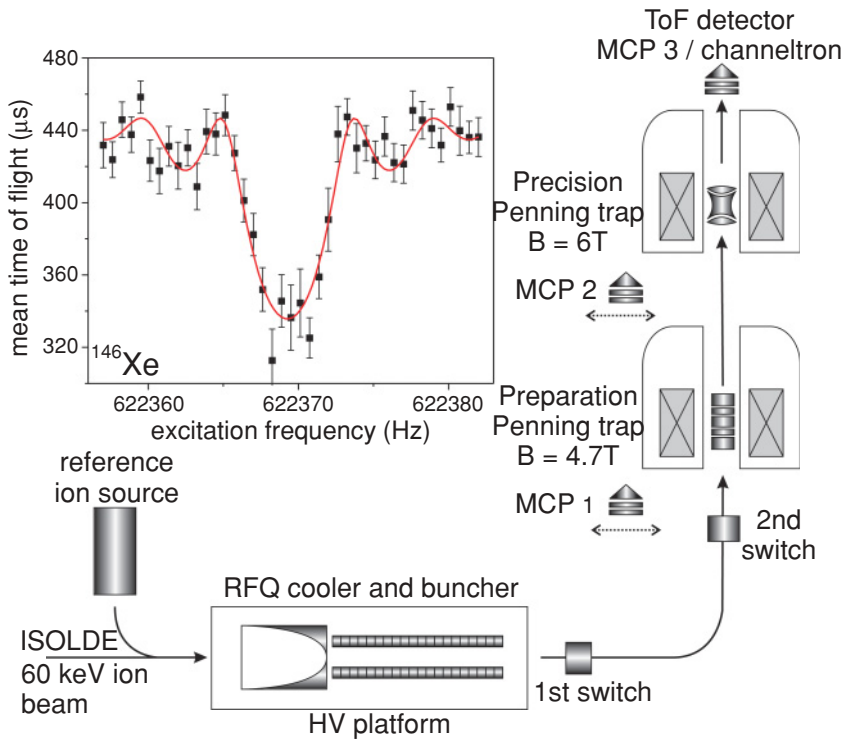

FIG. 1. (Color online) Sketch of the ISOLTRAP setup. The ions coming from ISOLDE are stopped in a linear RFQ and transported to the two Penning traps, where the mass is measured with the time-of-flight ion-cyclotron resonance method. Inset: Time-of-flight resonance curve of ^{146}Xe with an excitation time of 200 ms. The solid line is a fit of the expected line shape [18] to the data points.

The ion bunch from the preparation trap is transported to the hyperbolic precision Penning trap where the mass m of the ion is determined by the measurement of the cyclotron frequency $\nu_c = qB/(2\pi m)$, where q is the charge state of the ion and B the magnetic field strength. Inside the Penning trap, the radial motion of the ions can be described as a superposition of a fast cyclotron motion and a slow magnetron motion. To measure ν_c, the time-of-flight detection technique is used [21]. To this end, the ions in the precision trap are excited to a magnetron radius of about 0.7 mm, before a cyclotron excitation with frequency ν_{rf} is applied to increase the radial kinetic energy. The frequency of this excitation is varied around ν_c, and the time of flight of the ions ejected toward a detector is recorded.

In resonance, i.e., for $\nu_{\mathrm{rf}} = \nu_c$, the radial ion motion is converted from pure magnetron motion to pure cyclotron motion (with the same radius). Therefore, the ions have more kinetic energy and after axial ejection arrive earlier at the detector. The resolving power is approximately proportional to the product of the cyclotron frequency ν_c and the excitation time T_{rf}. Typically, excitation times from 0.1 up to 1.2 s are used.

An example for a cyclotron resonance is shown in Fig. 1 (inset). The expected line shape [18] is fitted to the data points. For each measurement, the magnetic field is calibrated by the determination of the cyclotron frequency $\nu_{c,\mathrm{ref}}$ of a reference ion with a well-known mass m_{ref}. For the present experiment, ^{133}Cs was used. Taking into account the mass m_e of the electron, the resulting mass of the ion of interest is

$$m = \frac{\nu_{c,\mathrm{ref}}}{\nu_c}\,(m_{\mathrm{ref}} - m_e) + m_e. \qquad (1)$$

To avoid any influence from possible contaminations, a count-rate analysis as described in Ref. [22] was applied. In addition to the statistical uncertainty of each measurement, a relative mass-dependent uncertainty of $1.6 \times 10^{-10} \times (m - m_{\mathrm{ref}})/u$ and a residual uncertainty of 8×10^{-9} were added quadratically.

III. RESULTS

For each xenon isotope, two or three resonances were recorded. The third column of Table I shows the mean frequency ratios compared to the reference ^{133}Cs. In total, 11 isotopes of xenon were measured, seven of them ($^{137-139}$Xe, ^{142}Xe, and $^{144-146}$Xe) directly for the first time. The masses of $^{144-146}$Xe have never been measured to date. The deduced frequency ratios were included into an evaluation in order to produce new mass excess values, which are compared with the literature values of the Atomic-Mass Evaluation 2003 [25] in Table I.

The mass of ^{136}Xe was recently measured with a very low mass uncertainty of only 11 eV [24] in a cryogenic Penning trap and served as a cross-check to confirm the reliability of ISOLTRAP. In addition, in the AME2003, the mass of ^{137}Xe is coupled to the mass of ^{136}Xe through a (n, γ) reaction with an uncertainty of only 110 eV [25], therefore the mass of this isotope turned out to be a second cross-check for our measurements. Both values are included in Table I, and our results are in very good agreement with these calibration points.

The masses of ^{140,141,143}Xe were recently measured at the cooler-storage ring ESR at GSI [23]. These measurements were performed in the isochronous mode to address short-lived nuclei, and mass uncertainties of ∼120 keV have been achieved. Whereas the mass excess values for ^{140,143}Xe agree within one σ with our measurements, our value for ^{141}Xe is roughly 2.5σ away from the result of the ESR measurement.

Figure 3 shows a comparison of our data with the literature values and the values from the ESR. Before our measurement, the AME2003 values for $^{138-142}$Xe were mainly determined by Q_β measurements in the decay of Cs [26–28]. Our results increase the precision of these masses by a factor of 10–40. Only for ^{138}Xe, a larger deviation from the mean literature value is observed. The result of Monnand *et al.* [28] deviates more than 4σ from our value. But it is known that data from Q_β measurements often underestimate the Q values because of missing levels in the daughter nuclide, thus providing more

TABLE I. Frequency ratios $r = \nu_{c,\mathrm{ref}}/\nu_c$, relative mass uncertainties $\delta m/m$, and mass excesses of the measured xenon isotopes Δ resulting from an evaluation including the new frequency ratios, the results from the measurement at the GSI experimental storage ring (ESR) Δ_{ESR} [23], and the literature values Δ_{Lit} from the AME2003 [25]. The measurement of Redshaw *et al.* [24] for ^{136}Xe is already included in the evaluation for the literature values. Extrapolated mass excess values are marked with ♯. The reference ion was $^{133}Cs^+$ with $m(^{133}\mathrm{Cs}) = 132.905451932(23)$ u [25].

A	$T_{1/2}$	$r = \nu_{c,\mathrm{ref}}/\nu_c$	$\delta m/m$	Δ (keV)	Δ_{ESR} (keV)	Δ_{Lit} (keV)
136	Stable	1.0225827874(143)	1.4×10^{-8}	−86429.8(1.8)	–	−86429.15(0.01)
137	3.8 min	1.0301426589(147)	1.5×10^{-8}	−82382.2(1.8)	–	−82383.37(0.11)
138	14.08 min	1.0376862793(260)	2.6×10^{-8}	−79975.1(3.3)	–	−80150(40)
139	39.68 s	1.0452454557(175)	1.8×10^{-8}	−75644.6(2.1)	–	−75644(21)
140	13.60 s	1.0527910833(189)	1.9×10^{-8}	−72986.5(2.3)	−72870(121)	−72990(60)
141	1.73 s	1.0603539448(234)	2.3×10^{-8}	−68197.3(2.9)	−68521(127)	−68330(90)
142	1.22 s	1.0679020930(219)	2.2×10^{-8}	−65229.7(2.7)	–	−65480(100)
143	511 ms	1.0754668738(379)	3.8×10^{-8}	−60202.9(4.7)	−60253(124)	−60450♯(200♯)
144	388 ms	1.0830179539(432)	4.3×10^{-8}	−56872.3(5.3)	–	−57280♯(300♯)
145	188 ms	1.0905855815(896)	9.0×10^{-8}	−51493(11)	–	−52100♯(300♯)
146	146 ms	1.098138336(198)	2.0×10^{-7}	−47955(24)	–	−48670♯(400♯)

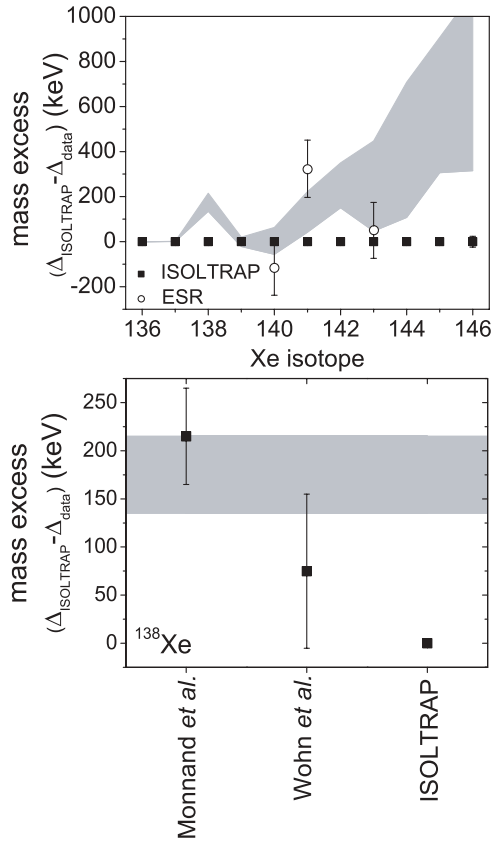

FIG. 3. (Top): Differences between the ISOLTRAP mass excess values and the values from the AME2003 compilation [25] (grey shaded region) and the results from the ESR at GSI [23] (open circles). (Bottom): Mass excess difference for ^{138}Xe compared with Q_β measurements [26,28]. The uncertainties of the ISOLTRAP measurements are smaller than the size of the symbols.

bound masses. However, no obvious reason could be found in this case. On the other hand, the measurements of Wohn *et al.* [26] lead to a mass excess for ^{138}Xe of −80056(80) keV, which agrees with the present results (see Fig. 3, bottom).

IV. DISCUSSION

The masses deduced for xenon isotopes reveal some interesting new information. Figure 4 shows the two-neutron separation energies S_{2n} for this region. Those for xenon, including the new values for $^{138-143}$Xe and the first measurements for $^{144-146}$Xe, behave rather smoothly. This smoothness is in contrast to the heavier chains, where deformation sets in around $N = 90$ and S_{2n} values flatten: as Z decreases, xenon is the first chain to show such smoothness.

Double differences of binding energies can be used to isolate particular interactions and are a much more sensitive indicator of structure. In particular, one specific double difference isolates the proton-neutron interaction of the last two protons with the last two neutrons, $\delta V_{pn}(Z, N)$. It is defined for even-even and even-odd nuclei, respectively,

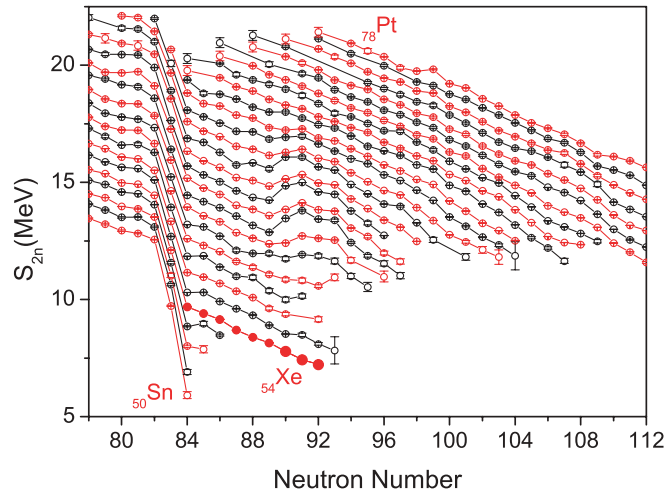

FIG. 4. (Color online) Two-neutron separation energies (S_{2n}) for Sn-Pt isotopes with $N = 78$–112 [25]. Red data points are for even-Z nuclides, black are for odd-Z nuclides. The new xenon data from this work are represented by the solid circles. The larger points are for the nuclei $^{144-146}$Xe for which no mass information was known.

by [29]

$$\delta V_{pn}^{ee}(Z, N) = \tfrac{1}{4}[(B_{Z,N} - B_{Z,N-2}) - (B_{Z-2,N} - B_{Z-2,N-2})],$$

$$\delta V_{pn}^{eo}(Z, N) = \tfrac{1}{2}[(B_{Z,N} - B_{Z,N-1}) - (B_{Z-2,N} - B_{Z-2,N-1})],$$

where B is the binding energy.

Each δV_{pn} value requires four binding energies, for nuclei with atomic number Z and $Z - 2$. The measured xenon masses improve δV_{pn} values for barium isotopes. These are shown in Fig. 5, where the new values obtained from the present data are shown as solid symbols in the upper and lower panels. We note that there are considerable changes with respect to the older values as can be seen by comparing the old and new mass excesses in Table I.

The new δV_{pn} values for the even-Z and odd-N isotopes (top panel) are the most interesting. The barium values show a pattern that resembles a parabolic trend. This behavior is unique in this region and only occurs in one other, a fact that may give a clue to its physical origin and possibly a new signature of structure. The only other region where such behavior appears is located around ^{224}Ra, whose δV_{pn} values are shown in the middle panel of Fig. 5 [30]. The similarity is striking. Both parabolas appear just after a closed neutron shell for nuclei whose proton number is six above a major shell closure.

This, however, is not the only similarity in these two regions: both are the best established regions of nuclei with strong octupole correlations [4] and exhibit the characteristic signatures of such correlations, namely, low-lying 1^- and 3^- states, an interleaving of positive- and negative-parity states in rotational bands at high spin, and enhanced $E1$ and $E3$ transition rates. Also, the inclusion of an octupole degree of freedom improves considerably the agreement between measured and calculated masses [7,8]. These data are summarized comprehensively in Ref. [4]; see especially Figs. 13 and 14 of that reference for the systematics of the 1^- and 3^- states, Fig. 17 for interleaved alternating parity

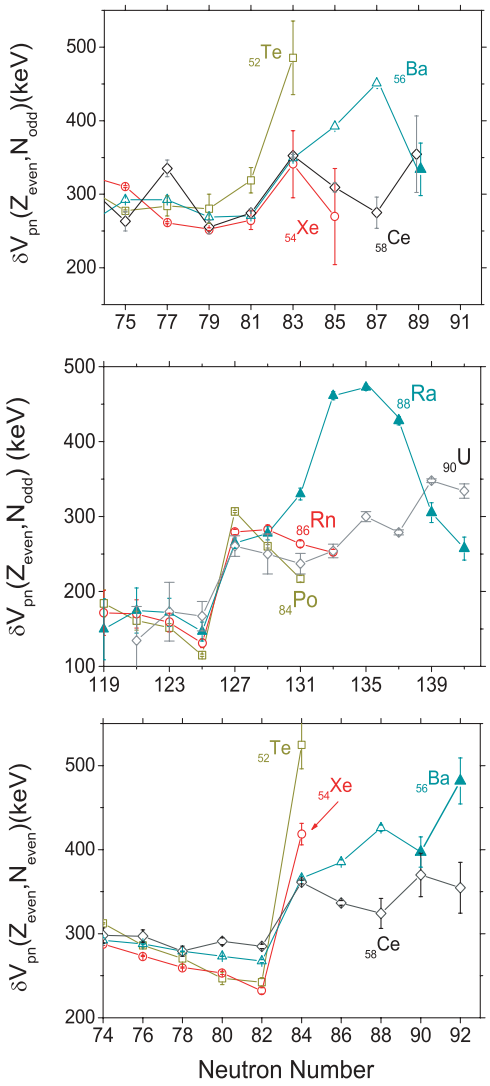

FIG. 5. (Color online) Empirical δV_{pn} values. (Top): Even-odd values for the barium region. The solid triangle represents the first extracted $\delta V_{pn}(^{145}\mathrm{Ba})$. (Middle): Same figure for the radium region [30]. (Bottom): Same as top, but for even-even nuclei.

states, and Tables III and IV for $E1$ and $E3$ transition rate data.

It is predicted that both regions develop softness to octupole effects [4] because, in the context of a microscopic random-phase approximation (RPA) approach, octupole collectivity should occur in regions where the shell model features nearby orbits differing by one in the oscillator quantum number (that is, having opposite parity), orbital angular momenta differing by 3, and single-particle total angular momenta differing by 3 as well. This occurs in heavy nuclei where the mean field spin-orbit force introduces an intruder orbital into each major shell. As shown in Fig. 6, the relevant orbits for the barium and radium regions are indeed present, namely, $(1i_{13/2}, 2f_{7/2})$ and $(1j_{15/2}, 2g_{9/2})$, respectively. Since the degeneracy of the orbits in the heavier region is higher, the onset of octupole correlations occurs a little later in the neutron major shell for radium than it does in the barium region.

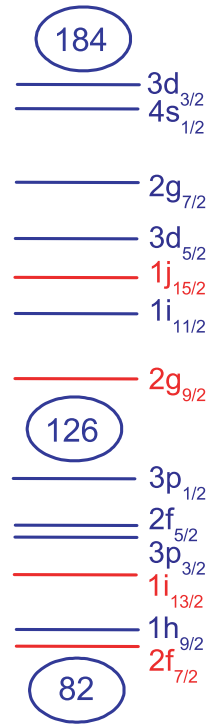

FIG. 6. (Color online) Colored version of Fig. 4 of Butler and Nazarewicz, the part from $N = 82$–184 [4], showing the single-particle levels for spherical nuclei.

In a sense, it is not surprising that evidence for octupole correlations appears in the context of mass measurements. Early calculations of the mass surface indeed showed a sensitivity to octupole correlations [31]. This was followed up by further studies [8,32] and octupole-correlation energy calculations [7].

Of course, it is one thing to see the effects of adding an octupole-octupole term in the collective Hamiltonian, but quite another to observe such effects directly in mass data. There are two reasons. First, current capabilities for microscopic mass calculations are on the order of 600 keV [33], which is somewhat larger than the expected octupole-correlation energies (see Fig. 7 of Ref. [4]). Second, such correlations will be superposed on presumably larger components from other structural effects such as the onset of quadrupole collectivity, likely to occur in the same regions. Nevertheless, octupole contributions to binding energies were noted in Refs. [7,8] although with the remark that they would be difficult to see directly in experimental binding energies or S_{2n} values. However, it seems likely that the distracting effects can be filtered out in δV_{pn} values. The fact that we indeed see a clear and unusual behavior in δV_{pn} values in two regions where octupole deformation occurs suggests that the onset of octupole deformation might be associated with anomalous empirical proton-neutron interaction strengths. Of course, this needs to be studied further, both theoretically and with additional mass measurements in regions of known octupole correlations.

The new δV_{pn} values have three further significant consequences: two connected to the relation between p-n interaction

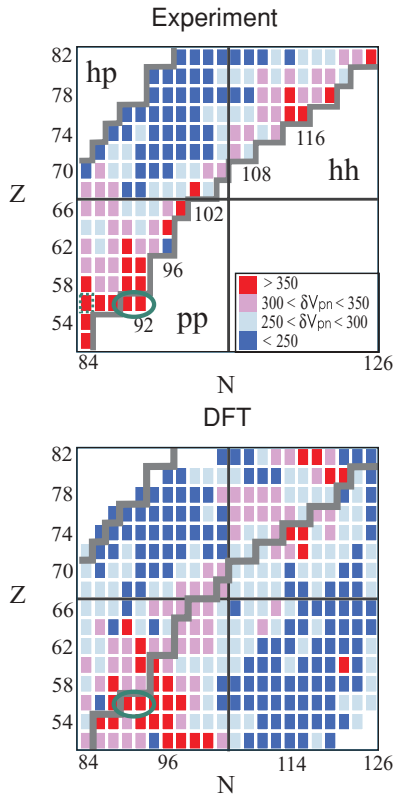

FIG. 7. (Color online) δV_{pn} values illustrated with colors for the $Z = 50$–82 and $N = 82$–126 shells. The top panel shows empirical values, for which the new and revised δV_{pn}(Ba) values are marked with a green ellipse. The bottom panel gives the DFT results taken from Ref. [13] and also marks the predictions for the two new barium nuclei that have been measured here.

strengths and the orbits occupied by the last valence nucleons, and one to recent microscopic calculations. Figure 7 illustrates the δV_{pn} values with a color scale for the $Z = 50$–82, $N = 82$–126 shells [11,12], in which the δV_{pn} increases from dark blue to red. The new δV_{pn}(Ba) results from this study are indicated by an elliptical frame at $N = 90$ and 92, and the revised δV_{pn} value is shown with a dotted frame at $N = 84$. This δV_{pn} value changed from 312 ± 10 keV (using the AME2003 [25] masses) to 365 ± 2 keV. All three new values are larger (red boxes).

This confirms the observations and physics arguments in Refs. [11,12] concerning the development of collectivity in different major shell regions. Cakirli and Casten [11] showed a correlation between the strength of the average p-n interaction and the growth rate of collectivity as measured, for example, by $R_{4/2}$, which is the energy ratio of the first 4^+ and the first 2^+ level. It was noticed [11,34] that collectivity grows most rapidly in particle-particle (p-p) ($Z = 50$–66, $N = 82$–104) and hole-hole (h-h) ($Z = 68$–82, $N = 104$–126) regions and slower in the hole-particle (h-p) ($Z = 68$–82, $N = 82$–126) region. The same result was observed in the empirical δV_{pn} values [11]. The δV_{pn} values, on average, are largest in the p-p region and are larger in the p-p and h-h than in the p-h region. The new δV_{pn}(Ba) values pertain to nuclei in the p-p quadrant and are indeed large (see Fig. 7 top), consistent with nuclei in the p-p quadrant with the faster growth of collectivity here.

There is a second aspect to these large δV_{pn} values that is of interest. Along a diagonal line from the bottom left to the top right in Fig. 7, the proton and neutron fractional filling ($f_p = N_p/32$ and $f_n = N_n/44$) is similar, $f_p \sim f_n$. Hence their orbits overlap the most, and large δV_{pn} values are expected [11,12]. This observation is reinforced by the new data.

Recent microscopic calculations using density functional theory (DFT) [13] can be tested with δV_{pn} values. Although these calculations only reproduce nuclear masses to an accuracy of $\sim$1 MeV, the binding energies they provide can be used to obtain theoretical δV_{pn} values. It has been shown [13] that generally (with some exceptions) the DFT reproduces empirical δV_{pn} values to quite high accuracy, on the order of $<$50 keV, and often considerably better. The reason is that the double difference embodied in δV_{pn} effectively filters out many contributions to binding and allows one to focus specifically on the ability of the DFT to predict valence p-n interactions. That is, by virtue of that double difference, one can inspect rather subtle but important correlations in the DFT wave functions. The present data allow an extension of such tests.

The DFT calculations also show a feature that is somewhat unexpected based on the above fractional filling argument, namely, the large δV_{pn} values for very neutron-rich Te-Ba nuclei. Mass measurements for δV_{pn} values of these nuclei would be an important test for these DFT calculations.

V. CONCLUSION

In summary, the masses of 11 neutron-rich xenon isotopes from $A = 136$ to $A = 146$ were measured by high-precision mass spectrometry, three of them ($^{144-146}$Xe) for the first time. The results provide information relevant to several nuclear structure studies. Previously, we pointed out a correlation of systematic δV_{pn} behavior with octupole effects [30] but also mentioned other possible sources of the empirical effect. Now we see similar behavior in another region (the barium nuclei), where octupole correlations are also known from other data. It is therefore suggestive that these anomalies in the δV_{pn} values may be correlated with octupole deformations but that it would be interesting to see if including such degrees of freedom in microscopic calculations improves their agreement with the δV_{pn} values, and the δV_{pn} values may serve as a signature of such shape softness. Of course, having such data does not replace more definite evidence from energy level sequences and transition rates, but it does have the potential advantage of providing the first evidence of such correlations in new regions where spectroscopic data are lacking.

In both the barium and radium regions, the peak in δV_{pn} values seems to occur at slightly lower neutron numbers than the maximum of the octupole correlations. Thus, as one moves experimentally toward neutron-rich nuclei in new regions far from stability, δV_{pn} values may even point to subsequent findings of octupole deformations. The precision of the present mass data and the filter provided by the double differences

in δV_{pn} can thus be combined to a valuable tool for the exploration of the nuclear landscape.

Moreover, the current results for the even-even nuclei provide new δV_{pn} values for barium, which have several consequences. They confirm the stronger interactions when the protons and neutrons are both filling the same halves of their respective shells, in particular when both are filling their shells to similar fractional degrees. In both cases, the last protons and neutrons occupy spatially similar orbits and hence exhibit stronger interactions. Figure 5 (bottom) reveals the δV_{pn} values for even Z and N. Measuring ^{144,146}Xe in this study allows us to extract the first δV_{pn} values for barium at $N = 90$ and 92 [similar to Fig. 5 (top) at $N = 89$]. Reference [30] mentions that the octupole effect in δV_{pn} clearly appears for the even-Z and odd-N but not for the even-Z and even-N nuclei. On the other hand, in this study, Fig. 5 (top and bottom panels) shows almost the same δV_{pn} values around $N \sim 88$. This result is a nice demonstration that measuring masses in possible octupole regions might be useful for further studies.

The new values support existing microscopic DFT calculations of δV_{pn} values. Although the absolute level of agreement of these calculations with known masses is only $\sim$1 MeV, the present results confirm that the DFT is, in fact, able to correctly account for important proton-neutron correlations in the microscopic wave functions that are critical to the evolution of nuclear structure with N and Z. Clearly, further mass measurements that could provide tests of the DFT calculations in the currently unknown region of neutron-rich isotopes of Te-Gd nuclei (see Fig. 7) would be quite valuable.

ACKNOWLEDGMENTS

We are grateful to the members of the ISOLDE technical and target groups for their support, particulary E. Noah, L. Penescu, and Th. Stora. This work was supported by the German Federal Ministry for Education and Research (BMBF) (06GF186I, 06MZ215), Helmholtz Association for National Research Centers (VH-NG-037), US Department of Energy (DE-FG02-91ER-40609), the French IN2P3, Turkish Atomic Energy Authority (TAEK) O4K120100-4, the EU FP6 programme (MEIF-CT-2006-042114, the EURISOL DS project/515768 RIDS), the ISOLDE collaboration, and the Max Planck society. R. Casten acknowledges support by the Mercator program at the University of Köln (Ko. 142/112-1) of the DFG.

[1] D. Lunney *et al.*, Rev. Mod. Phys. **75**, 1021 (2003).
[2] K. Blaum, Phys. Rep. **425**, 1 (2006).
[3] C. Thibault *et al.*, Phys. Rev. C **12**, 644 (1975).
[4] P. A. Butler and W. Nazarewicz, Rev. Mod. Phys. **68**, 349 (1996).
[5] Special issue of the International Journal of Mass Spectrometry, edited by L. Schweikhard and G. Bollen (Elsevier, Amsterdam, 2006), Vol. 251/2–3, pp. 85–312.
[6] M. Mukherjee *et al.*, Eur. Phys. J. A **35**, 1 (2008).
[7] W. Nazarewicz, P. Olanders, I. Ragnarsson, J. Dudek, G. A. Leander, P. Möller, and E. Ruchowska, Nucl. Phys. **A429**, 269 (1984).
[8] G. A. Leander *et al.*, Nucl. Phys. **A388**, 452 (1982).
[9] R. B. Cakirli, R. F. Casten, R. Winkler, K. Blaum, and M. Kowalska, Phys. Rev. Lett. **102**, 082501 (2009).
[10] W. R. Phillips, I. Ahmad, H. Emling, R. Holzmann, R. V. F. Janssens, T. L. Khoo, and M. W. Drigert, Phys. Rev. Lett. **57**, 3257 (1986).
[11] R. B. Cakirli and R. F. Casten, Phys. Rev. Lett. **96**, 132501 (2006).
[12] R. B. Cakirli, D. S. Brenner, R. F. Casten, and E. A. Millman, Phys. Rev. Lett. **94**, 092501 (2005).
[13] M. Stoitsov, R. B. Cakirli, R. F. Casten, W. Nazarewicz, and W. Satula, Phys. Rev. Lett. **98**, 132502 (2007).
[14] S. Goriely, S. Hilaire, M. Girod, and S. Péru, Phys. Rev. Lett. **102**, 242501 (2009).
[15] E. Kugler, Hyperfine Interact. **129**, 23 (2000).
[16] L. Penescu *et al.*, Nucl. Instrum. Methods B **266**, 4415 (2008).
[17] H. Frånberg *et al.*, Nucl. Instrum. Methods B **266**, 4502 (2008).
[18] M. König *et al.*, Int. J. Mass Spectrom. Ion Process. **142**, 95 (1995).
[19] F. Herfurth *et al.*, Nucl. Instrum. Methods A **469**, 254 (2001).
[20] G. Savard *et al.*, Phys. Lett. **A158**, 247 (1991).
[21] G. Gräff *et al.*, Z. Phys. A **297**, 35 (1980).
[22] A. Kellerbauer *et al.*, Eur. Phys. J. D **22**, 53 (2003).
[23] B. Sun *et al.*, Nucl. Phys. **A812**, 1 (2008).
[24] M. Redshaw, E. Wingfield, J. McDaniel, and E. G. Myers, Phys. Rev. Lett. **98**, 053003 (2007).
[25] G. Audi, A. H. Wapstra, and C. Thibault, Nucl. Phys. **A729**, 337 (2003).
[26] F. K. Wohn and W. L. Talbert, Phys. Rev. C **18**, 2328 (1978).
[27] M. Groß *et al.*, Nucl. Instrum. Methods A **311**, 512 (1992).
[28] E. Monnand *et al.*, Nucl. Phys. **A195**, 192 (1972).
[29] J.-Y. Zhang, R. F. Casten, and D. S. Brenner, Phys. Lett. **B227**, 1 (1989).
[30] D. Neidherr *et al.*, Phys. Rev. Lett. **102**, 112501 (2009).
[31] P. Möller, Nucl. Phys. **A192**, 529 (1972).
[32] P. Möller and J. R. Nix, Nucl. Phys. **A361**, 117 (1981).
[33] S. Goriely, N. Chamel, and J. M. Pearson, Phys. Rev. Lett. **102**, 152503 (2009).
[34] D. S. Brenner, J. Radiol. Nucl. Chem. **243**, 31 (2000).